ACADEMIC PRESS

Available online at www.sciencedirect.com
SCIENCE DIRECT®

Journal of Catalysis 218 (2003) 178–190

JOURNAL OF CATALYSIS

www.elsevier.com/locate/jcat

DFT studies for cleavage of C–C and C–O bonds in surface species derived from ethanol on Pt(111)

R. Alcalá, M. Mavrikakis, and J.A. Dumesic *

Department of Chemical Engineering, University of Wisconsin-Madison, Madison, WI 53706, USA

Received 15 November 2002; revised 4 March 2003; accepted 5 March 2003

Abstract

Results from self-consistent periodic DFT calculations were used to study the relative stabilities and reactivities of surface species on Pt(111) derived by subsequent removal of hydrogen atoms from ethanol. Within each C_2OH_x isomeric set, the lowest energy surface species (with respect to gaseous ethanol and clean Pt(111) slabs) are ethanol, 1-hydroxyethyl (CH_3CHOH), 1-hydroxyethylidene (CH_3COH), acetyl (CH_3CO), ketene (CH_2CO), ketenyl (CHCO), and CCO species. The energies of these species are −27, −28, −55, −84, −82, −88, and −53 kJ/mol, respectively, where the corresponding H atoms removed from ethanol are adsorbed on separate Pt(111) slabs. Transition states for C–C and C–O bond cleavage reactions were calculated for the most stable intermediates and for intermediates leading to exothermic bond cleavage reactions. A linear correlation between the energies of transition state and the energies of corresponding surface species was used to estimate transition-state energies of remaining reaction intermediates. The 1-hydroxyethylidene (CH_3COH) species has the lowest energy transition state (42 kJ/mol) for C–O bond cleavage, and the adsorbed ethylidyne (CCH_3) and hydroxyl product species lead to a favorable energy change for this C–O bond cleavage reaction (−38 kJ/mol). The ketenyl (CHCO) species has the lowest energy transition state (4 kJ/mol) for C–C bond cleavage, and the adsorbed CO and methylidyne (CH) product species lead to a very exothermic energy change for this reaction (−144 kJ/mol). Results from DFT calculations, combined with transition state theory, predict that the rate constant for C–C bond cleavage in ethanol is faster than for C–O bond cleavage on Pt(111) at temperatures higher than about 550 K. In addition, the calculated value of the rate constant for C–C bond cleavage in ethanol is predicted to be much higher than for C–C bond cleavage in ethane on Pt(111). Similarly, the rate of C–O bond cleavage in ethanol is predicted to be much higher than for C–O bond cleavage in carbon monoxide on Pt(111).

Keywords: DFT; Platinum; Ethanol; Decomposition

1. Introduction

Hydrogen fuel cells are promising devices for generation of power, since they operate at relatively low temperatures (e.g., 350 K) and produce only water as a by-product. While current methods for producing hydrogen require high-temperature steam reforming of nonrenewable hydrocarbon feed stocks, greater environmental benefits of operating hydrogen fuel cells would be realized if the hydrogen fuel could be produced from renewable resources, such as biomass. In particular, even though CO_2 would be produced as a by-product from reforming of biomass resources, this CO_2 would be fixed and stored by plant biomass grown subsequently for further hydrogen production. In addition, oxygenated hydrocarbons derived from renewable resources are relatively nontoxic and easy to store and handle. In this respect, it has recently been reported that hydrogen can be produced at relatively low temperatures (e.g., 500 K) over supported Pt catalysts by aqueous-phase reforming of biomass-derived oxygenated hydrocarbons (such as methanol, ethylene glycol, glycerol, sorbitol, and glucose) [1].

The generation of H_2 and CO_2 by reforming at low temperatures is controlled by selectivity considerations, since the subsequent reaction of H_2 and CO or CO_2 to form alkanes (C_nH_{2n+2}) and water is highly favorable at these low temperatures. For example, the equilibrium constant at 500 K for the conversion of CO_2 and H_2 to give methane

* Corresponding author: Department of Chemical Engineering, 1415 Engineering Drive, Madison, WI 53715, USA.
E-mail address: dumesic@engr.wisc.edu (J.A. Dumesic).

0021-9517/03/$ – see front matter
doi:10.1016/S0021-9517(03)00090-3

by the following reaction is of the order of 10^{10} per mole of CO_2:

$$CO_2 + 4H_2 \leftrightarrow CH_4 + 2H_2O.$$

In addition, an oxygenated hydrocarbon can form undesirable alkanes via cleavage of the C–O bond, followed by hydrogenation. Thus, the production of hydrogen by reforming of oxygenated hydrocarbons at low temperatures requires selective cleavage of C–C bonds compared to C–O bonds.

In the present paper, we report results from periodic density functional theory (DFT) calculations to probe the nature of surface intermediates that may be formed on Pt(111) by the decomposition of ethanol. In addition, we probe transition states for cleavage of C–C and C–O bonds in these intermediates adsorbed on Pt(111) to identify and compare the most favorable pathways for cleavage of C–C and C–O bonds during ethanol decomposition on Pt-based catalysts. The DFT calculations of the present work are an extension of work reported previously for ethanol decomposition on Pt [2]. We choose ethanol for study since this molecule is a simple oxygenated hydrocarbon containing a C–C bond. In addition, ethanol can be produced by fermentation from renewable resources. Furthermore, from a fundamental point of view, alcohols are among the most extensively studied oxygenated hydrocarbons on transition metals.

Various surface science studies have addressed the reactivities of alcohols on Pt(111) surfaces under ultrahigh vacuum conditions at different temperatures. Methanol and ethanol desorption was reported at low temperatures (194 and 213 K, respectively) [3]. Vannice et al. reported isopropanol dehydrogenation and acetone desorption at temperatures between 190 and 230 K [4], and Sexton et al. reported 10% decomposition of C_1–C_4 alcohol monolayers near 200 K and formation of CO, H_2, and surface C [5]. Alcohol decomposition reactions were shown to occur on surface defect sites [6]. Ethanol dehydrogenation forming acetaldehyde was reported at higher temperatures (295 K) followed by decomposition and formation of C_xH_y species [7].

The results from the aforementioned studies suggest that C–C and C–O bond cleavage reactions do not occur at low temperatures (< 200 K) on Pt(111). However, cleavage of the C–C bond in ethanol at low temperatures (200–300 K) has been reported on Pt(331) [8]. In addition, C–C and C–O bond cleavage reactions were reported for acetaldehyde decomposition on Pt(S)–[6(111) × (100)] at 290 and above 300 K, respectively [9]. Furthermore, Schauermann et al. report that catalytic activity for C–O bond cleavage in methanol is significantly enhanced on defect sites compared to the reactivity of Pd(111) surfaces [10]. These experimental results point to the structure sensitivity of alcohol reactions on noble metal catalysts, particularly Pt. However, DFT calculations on Pt(111) provide a starting point to probe ethanol C–C and C–O bond cleavage reactions on supported Pt catalysts [2]. Ethanol conversion on these supported Pt catalysts at temperatures above 490 K resulted in higher selectivity for C–C bond cleavage products (methane and CO) compared to C–O bond cleavage product (ethane) selectivity.

2. Methods

Self-consistent periodic calculations [11] based on gradient-corrected density functional theory were conducted for two-layer Pt(111) slabs. The 2×2 two-layer unit cell, containing a total of 8 metal atoms, was repeated periodically, with four equivalent layers of vacuum between any two successive metal slabs. Total energy calculations were performed using DACAPO [12]. Ionic cores are described by ultrasoft pseudopotentials [13] and the Kohn–Sham one-electron valence states are expanded in a basis of plane waves with kinetic energies below 25 Ry. The surface Brillouin zone is sampled at 18 special k points. The exchange-correlation energy and potential are described by the Perdew–Wang 1991 (PW91) generalized gradient approximation (GGA) [14,15]. The self-consistent density is determined by iterative diagonalization of the Kohn–Sham Hamiltonian, Fermi population of the Kohn–Sham states ($k_BT = 0.1$ eV) and Pulay mixing of the resulting electronic density [16]. All reported binding energies are calculated using the PW91 functional, and these energies have been extrapolated to $k_BT = 0$ eV.

Adsorption occurs on one side of the slab. The metal atoms were fixed in their bulk-terminated positions and all adsorbate atoms were allowed to relax. The lattice constant used in the calculations was 4.00 Å [17,18], compared to the experimental bulk lattice constant of 3.93 Å [19]. The energy change for dissociative adsorption of H_2 is calculated to be -86 kJ/mol. This value is in agreement with reported experimental results on supported platinum catalysts and platinum powder (-90 kJ/mol) [20,21]. Different sites were explored (e.g., top, bridge, and threefold) to find the lowest energy-binding mode for each species. Most species follow gas-phase bond order rules, wherein C is tetravalent and O is divalent, except for a few exceptions (that will be addressed in the discussion section).

Convergence with respect to lateral unit cell dimensions was confirmed on 3×3 two-layer unit cells, where the surface Brillouin zone is sampled at six special k points. Convergence with respect to number of metal layers and surface relaxation was confirmed on 2×2 three-layer unit cells with relaxation of top layer metal atoms. Binding energies of dehydrogenated ethanol species (and transition states) on two-layer 2×2 slabs were 0–20 kJ/mol *larger* compared to binding energies on two-layer 3×3 and three-layer 2×2 slabs with relaxation of the top metal layer. Gas-phase calculations were carried out in a $15.00 \times 15.00 \times 15.75$ Å unit cell and the Brillouin zone is sampled at one k point. The magnetic moments of gas-phase radical species were optimized during the geometry optimizations. Transition states are estimated

using constrained optimizations, where the bond length representing the reaction coordinate is constrained and all other degrees of freedom are optimized. The transition states are characterized by the configuration with the highest energy along the reaction coordinate and a transition from repulsive to attractive forces along the constrained bond [17,22,23]. This procedure for determining the transition state of relatively large adsorbates has proven to yield energy barriers of reasonable accuracy, compared to more rigorous methods, such as the nudged elastic band method [18,24–26].

3. Results

3.1. Gas-phase intermediates

Gas-phase species are shown in Fig. 1 (species 1–6) including geometric parameters, i.e., bond lengths and angles. The C–C and C–O bond lengths in ethanol (species 1) are 1.52 and 1.43 Å, respectively, and the CCO bond angle is 113° from DFT calculations. The bond lengths and CCO angle are in agreement with experimental values (1.51 and 1.43 Å, and 108°, respectively) [27]. The geometric parameters of acetaldehyde and ethylene oxide (species 2 and 3) are in agreement with experimental results (±0.02 Å and ±0.2°) [27]. For the hydroxyethylene species (CH_2CHOH; species 4), the calculated lengths of C–C and C–O bonds (1.34 and 1.37 Å, respectively) and the CCO bond angle (127°) are in agreement with reported values from other theoretical calculations (1.33, 1.37 Å and 122°, respectively) [28]. Ketene (CH_2CO; species 5) has C=C and C=O double bonds, and the lengths of these bonds (1.31 and 1.18 Å, respectively) are in agreement with reported bond lengths (1.32 and 1.16 Å, respectively) [27]. The experimental ketene CCO bond angle was not reported.

Values of electronic energies (with respect to gas-phase ethanol) of gas-phase intermediates derived from ethanol are shown in Table 1. These values correspond to the lowest energies from spin-polarized calculations, leading to values of magnetic moments usually equal to 0 or 1. The following species have magnetic moments equal to 2: O, C, CH_2, CC, CH_3CH, CCO, CCHOH, CHCHO, and $CHCH_2OH$.

3.2. Surface dehydrogenation reactions

Adsorption geometries of surface intermediates derived by dehydrogenation of ethanol on Pt(111) ($\theta = 1/4$ ML) are shown in Fig. 2 (species 1–24). Values of electronic energies (with respect to gas-phase ethanol and clean Pt slabs) of surface intermediates and products of C–O and C–C bond cleavage reactions are shown in Table 2. The binding modes of these species are listed in Table 3, where we have used the nomenclature $\eta_i \mu_j$ to designate that i atoms of the adsorbate are bonded to j-metal atoms on the surface. Bond lengths of these species are also listed in Table 3.

The calculated binding energy of ethanol on Pt(111) is 27 kJ/mol. Similar values have been reported for the adsorption of methanol, n-propanol, and isopropanol on

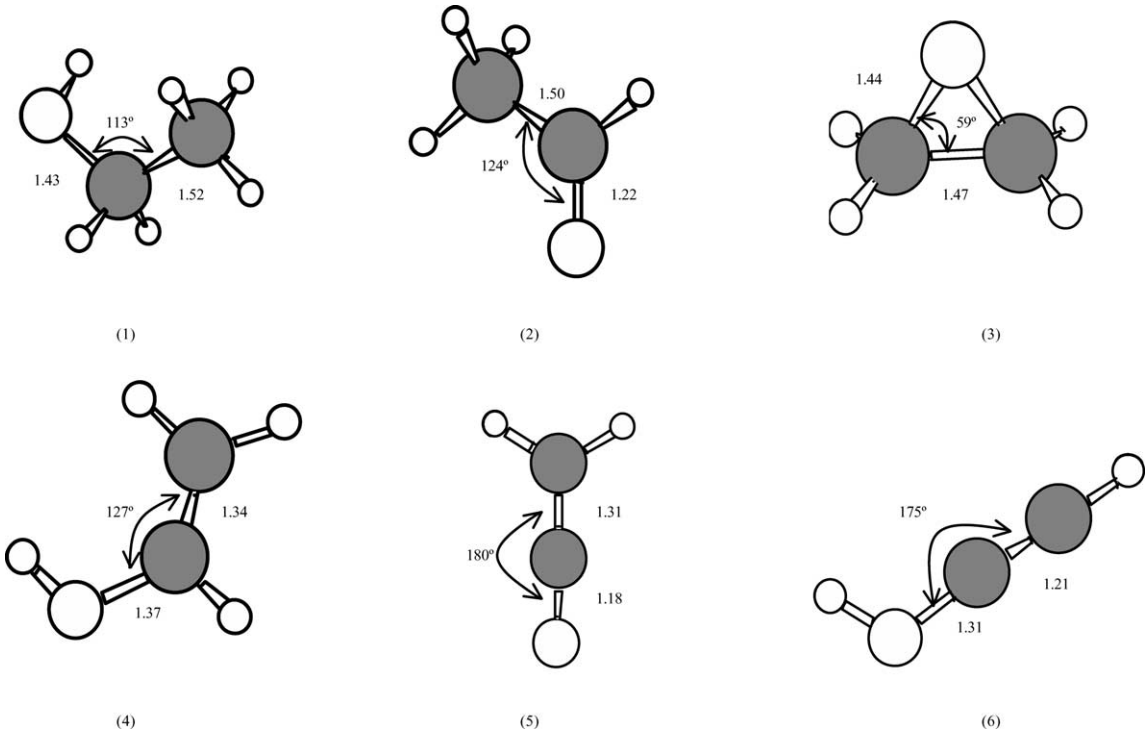

Fig. 1. Gas-phase species: (1) ethanol, (2) acetaldehyde, (3) ethylene oxide (CH_2CH_2O), (4) hydroxyethylene (CH_2CHOH), (5) ketene (CH_2CO), and (6) hydroxyacetylene (CHCOH). Bong lengths are given in Å and angles in degrees. The gray medium circles represent C atoms, white medium circles represent O atoms, and the small white circles represent H atoms.

Table 1
Electronic energies (kJ/mol) from DFT calculations for gas-phase reactions relative to gas-phase ethanol[a]

Intermediate (stoichiometry)	Gas-phase reactions[a]		
	Intermediate	C–O cleavage	C–C cleavage
Ethanol (CH_3CH_2OH)	0	420	357
Ethoxy (CH_3CH_2O)	174	604	260
1-Hydroxyethyl (CH_3CHOH)	131	617	481
2-Hydroxyethyl (CH_2CH_2OH)	172	340	570
Acetaldehyde (CH_3CHO)	13	801	378
Ethylene oxide (CH_2CH_2O)	111	524	472
1-Hydroxyethylidene (CH_3COH)	234	761	547
Hydroxyethylene (CH_2CHOH)	47	544	693
2-Hydroxyethylidene ($CHCH_2OH$)	366	544	789
Acetyl (CH_3CO)	130	945	243
Formylmethyl (CH_2CHO)	148	728	590
($CHCH_2O$)	283	728	692
1-Hydroxyvinyl (CH_2COH)	252	663	759
2-Hydroxyvinyl (CHCHOH)	266	474	913
2-Hydroxyethylidyne (CCH_2OH)	496	663	862
Ketene (CH_2CO)	64	847	455
Formylmethylene (CHCHO)	349	659	810
(CCH_2O)	331	847	764
Hydroxyacetylene (CHCOH)	217	781	979
Hydroxyvinylidene (CCHOH)	504	781	985
Ketenyl (CHCO)	246	965	675
Formylmethylidyne (CCHO)	471	965	882
Hydroxyethynyl (CCOH)	485	1029	1051
(CCO)	424	1213	748

The DFT H_2 heat of adsorption on Pt(111) is 86 kJ/mol.

[a] Excess H adsorbed on a separate slab; bond cleavage products are calculated separately (i.e., at infinite separation).

Pt(111) [18,29]. The ethanol molecule, shown in Fig. 2 (species 1), binds to the metallic surface through the lone pair electrons on oxygen, and the O–Pt distance is 2.56 Å.

Removal of an H atom from ethanol leads to the formation of three possible surface intermediate species. The most stable of these surface species is 1-hydroxyethyl (CH_3CHOH), and it is shown in Fig. 2 (species 3). The reaction energy change for the formation of 1-hydroxyethyl (CH_3CHOH plus surface H) is −28 kJ/mol relative to gas-phase ethanol. The 1-hydroxyethyl (CH_3CHOH) and 2-hydroxyethyl (CH_2CH_2OH) species bind on atop sites through C atoms. The least stable surface species in this isomer set is the ethoxy (CH_3CH_2O) species, which binds on atop sites through the O atom. The O–Pt distance (2.05 Å) for this species indicates the formation of an O–Pt bond, compared to the longer O–Pt distance in adsorbed ethanol (2.56 Å). The O–Pt bond length in the ethoxy species is in agreement with the reported O–Pt bond length in adsorbed methoxy species (2.03 Å) [18].

The most stable surface species containing four H atoms is 1-hydroxyethylidene (CH_3COH). This species adsorbs on atop sites as shown in Fig. 2 (species 7). The reaction energy change for the formation of 1-hydroxyethylidene (CH_3COH plus two surface H atoms) is −55 kJ/mol relative to gas-phase ethanol. The C–Pt bond length (1.97 Å) is shorter than C–Pt bonds in other adsorbed molecules. In addition, the C–O bond length (1.31 Å) is between that of a single bond and a double bond. Acetaldehyde adsorbs across a bridge site. The C–O bond in acetaldehyde lengthens upon adsorption (from 1.22 to 1.35 Å), in agreement with findings for adsorption of formaldehyde (1.34 Å) on Pt(111) [18], and the

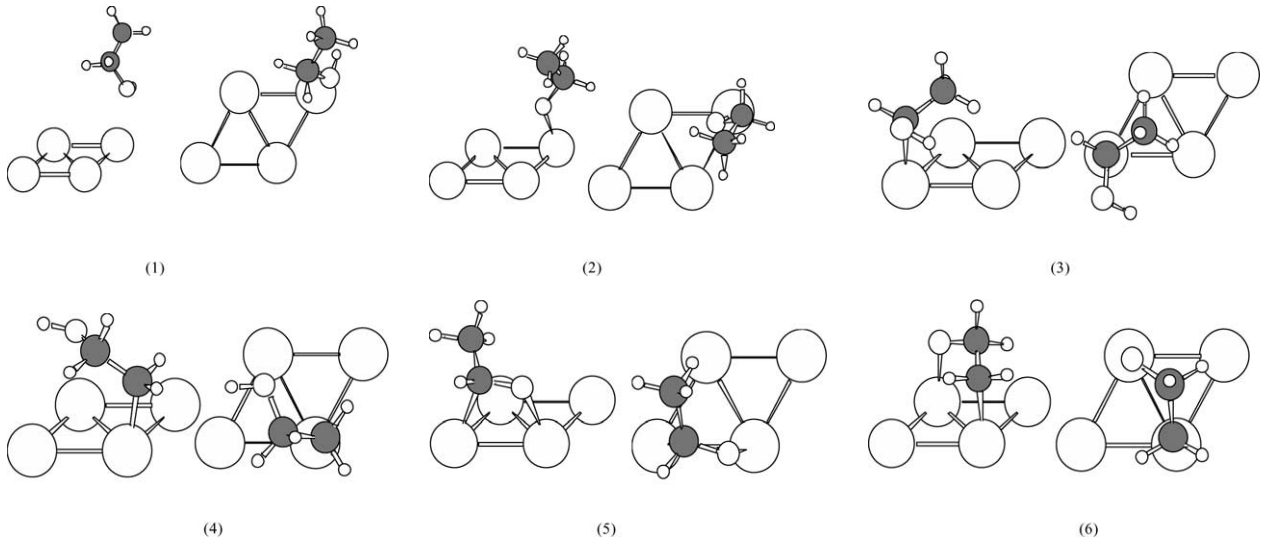

Fig. 2. Side and top views for surface intermediates: (1) ethanol, (2) alkoxy (CH_3CH_2O), (3) 1-hydroxyethyl (CH_3CHOH), (4) 2-hydroxyethyl (CH_2CH_2OH), (5) acetaldehyde, (6) ethylene oxide (CH_2CH_2O), (7) 1-hydroxyethylidene (CH_3COH), (8) hydroxyethylene (CH_2CHOH), (9) 2-hydroxyethylidene ($CHCH_2OH$), (10) acetyl (CH_3CO), (11) formylmethyl (CH_2CHO), (12) $CHCH_2O$, (13) 1-hydroxyvinyl (CH_2COH), (14) 2-hydroxyvinyl (CHCHOH), (15) hydroxyethylidyne (CCH_2OH), (16) ketene (CH_2CO), (17) formylmethylene (CHCHO), (18) CCH_2O, (19) hydroxyacetylene (CHCOH), (20) hydroxyvinilydene (CCHOH), (21) ketenyl (CHCO), (22) formylmethylidyne (CCHO), (23) hydroxyethynyl (CCOH), and (24) CCO. The large white circles represent Pt atoms, gray medium circles represent C atoms, white medium circles represent O atoms, and the small white circles represent H atoms.

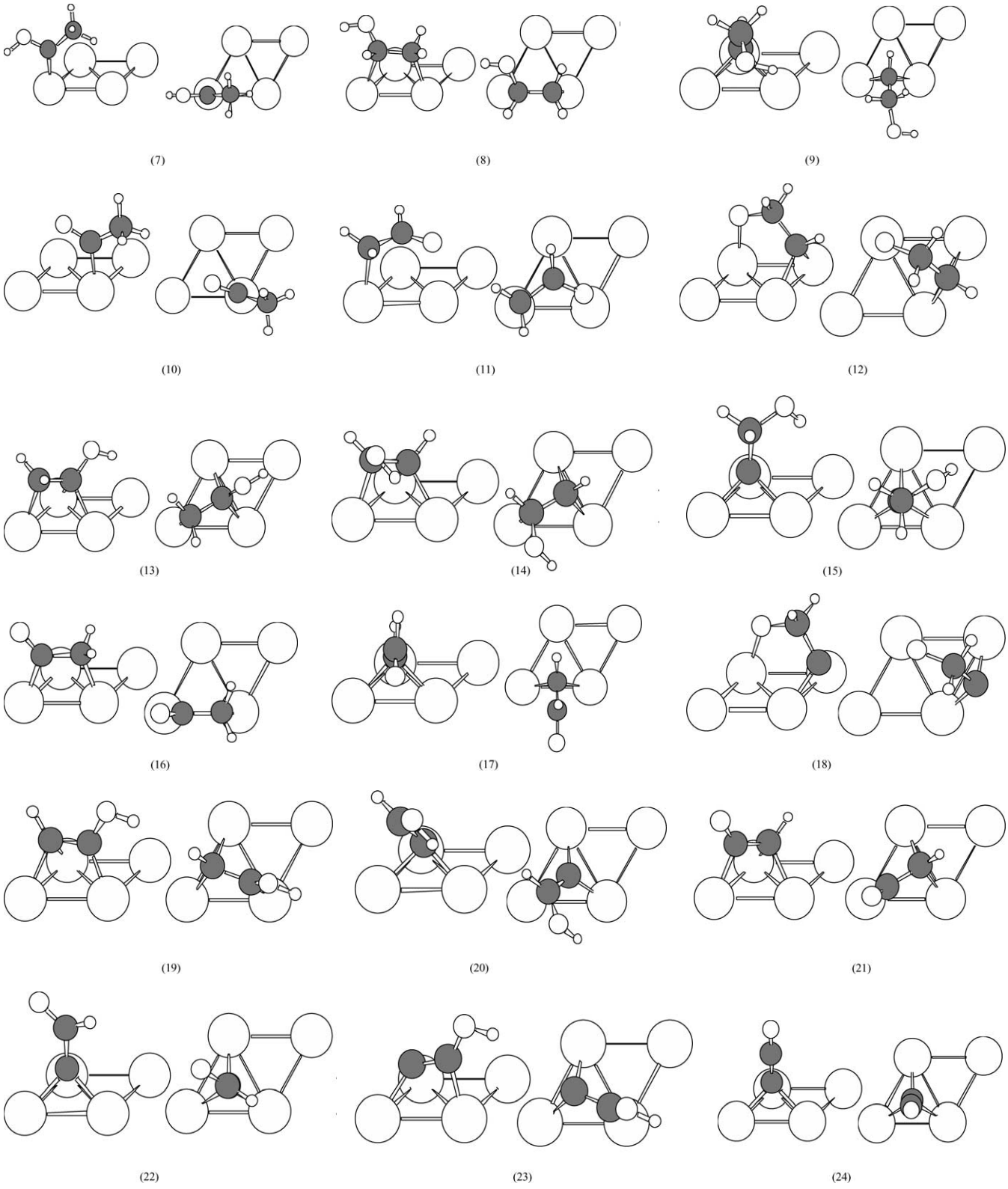

Fig. 2. Continued.

C and O atoms bind on neighboring atop sites. Ethylene oxide (CH_2CH_2O) is the most unstable species in this isomeric set. Upon adsorption, the gas-phase ring structure opens and the molecule binds on neighboring atop sites through the O and C atoms, forming an oxametallacycle intermediate [30] as shown in Fig. 2 (species 6).

The most stable adsorbed species containing three H atoms is the acetyl (CH_3CO) species, which adsorbs on atop

Table 2
Electronic energies (kJ/mol) from DFT calculations for surface reactions on Pt(111)[a] relative to gas-phase ethanol and clean slab(s)

Intermediate (stoichiometry)	Figs. 2, 4, and 5 species	Surface reactions[a]				
		Intermediate	C–O TS	C–O cleavage	C–C TS	C–C cleavage
Ethanol (CH_3CH_2OH)	1	**−27**	(126)	**35**		**17**
Ethoxy (CH_3CH_2O)	2	38		60		32
1-Hydroxyethyl (CH_3CHOH)	3	**−28**		50	(127)	**−12**
2-Hydroxyethyl (CH_2CH_2OH)	4	−1	192	**16**		37
Acetaldehyde (CH_3CHO)	5	−4		75	115	−31
Ethylene oxide (CH_2CH_2O)	6	14	(168)	41	157	52
1-Hydroxyethylidene (CH_3COH)	7	**−55**	42	**−38**	(71)	**−78**
Hydroxyethylene (CH_2CHOH)	8	−44	113	22		8
2-Hydroxyethylidene ($CHCH_2OH$)	9	1	(157)	22	(128)	−23
Acetyl (CH_3CO)	10	**−84**	135	**−14**	45	**−104**
Formylmethyl (CH_2CHO)	11	−30		47	97	−11
($CHCH_2O$)	12	30		47		−9
1-Hydroxyvinyl (CH_2COH)	13	−70	65	18	(93)	−58
2-Hydroxyvinyl ($CHCHOH$)	14	−48	(107)	35	(96)	−53
2-Hydroxyethylidyne (CCH_2OH)	15	−67	121	18		47
Ketene (CH_2CO)	16	**−82**	(85)	**42**	51	−84
Formylmethylene ($CHCHO$)	17	−34		60	(80)	−72
(CCH_2O)	18	83		**42**		62
Hydroxyacetylene ($CHCOH$)	19	−63		141	78	**−119**
Hydroxyvinylidene ($CCHOH$)	20	−61		141	118	18
Ketenyl ($CHCO$)	21	**−88**		**166**	4	**−144**
Formylmethylidyne ($CCHO$)	22	−42		**166**	(124)	−1
Hydroxyethynyl ($CCOH$)	23	37		273		−48
(CCO)	24	**−53**		**298**	84	**−74**

The DFT H_2 heat of adsorption on Pt(111) is 86 kJ/mol. Values in bold correspond to the lowest value within each isomeric set. Values in parentheses are estimated from the linear correlation plot in Fig. 6.

[a] Excess H adsorbs on a separate slab; bond cleavage products adsorb on separate slabs.

sites. The reaction energy change for the formation of adsorbed acetyl (CH_3CO) species (plus three surface H atoms) is −84 kJ/mol relative to gas-phase ethanol. The C–O bond length is 1.22 Å and is characteristic of a C=O double bond.

The most stable surface species containing two H atoms is ketene (CH_2CO), which adsorbs on a bridge site. The reaction energy change for the formation of adsorbed ketene (CH_2CO) species (plus four surface H atoms) is −82 kJ/mol relative to gas-phase ethanol. Ketene adsorbs through both C atoms on neighboring atop sites, as shown in Fig. 2 (species 16). The gas-phase ketene C=C double bond is lengthened from 1.31 to 1.49 Å upon adsorption.

The most stable surface species containing one hydrogen atom is the ketenyl (CHCO) species, and the reaction energy change for the formation of surface ketenyl (CHCO) species (plus five surface H atoms) from gas-phase ethanol is −88 kJ/mol. This reaction energy change of formation from ethanol is the most favorable of all surface intermediates studied. The ketenyl (CHCO) species adsorbs on a threefold Pt atom ensemble, as shown in Fig. 2 (species 21). The carbonyl C atom binds to atop sites and the other C atom binds to a bridge site.

3.3. Surface reactions involving cleavage of C–O and C–C bonds

To identify favorable surface intermediates for cleavage of C–O or C–C bonds, the energies of adsorption for all possible products of bond cleavage reactions were investigated on the Pt(111) surface. Changes in electronic energies corresponding to the formation of these C–O and C–C bond cleavage products relative to gas-phase ethanol and the clean Pt surface are listed in Table 2. The results from these calculations for adsorbed reaction products were used to guide the search for low-energy transition states for cleavage of C–O and C–C bonds. Accordingly, 6 routes for cleavage of the C–O bond were investigated, corresponding to adsorbed intermediates leading to low energy adsorbed products. Similarly, 9 routes for cleavage of the C–C bond were investigated, corresponding to adsorbed intermediates leading to low-energy adsorbed products, plus selected intermediates with less favorable reaction energetics. The geometries of transition states for these 15 bond cleavage routes are shown in Fig. 3 (species 1–15). Electronic energies and bond lengths corresponding to these transition states are listed in Tables 2 and 4, respectively.

Table 3
Bond lengths (Å) and binding modes from DFT calculations for intermediate surface species on Pt(111)

Intermediate	Fig. 2 species	Binding mode	O–Pt	C–Pt	C–O	C–C
CH_3CH_2OH	1		2.56	–	1.44	1.52
CH_3CH_2O	2	$\eta_1\mu_1$ (O)	2.05	–	1.42	1.52
CH_3CHOH	3	$\eta_1\mu_1$ (C)	–	2.18	1.40	1.51
CH_2CH_2OH	4	$\eta_1\mu_1$ (C)	–	2.13	1.44	1.50
CH_3CHO	5	$\eta_2\mu_2$ (C,O)	2.13	2.21	1.35	1.51
CH_2CH_2O	6	$\eta_2\mu_2$ (C,O)	2.05	2.10	1.39	1.51
CH_3COH	7	$\eta_1\mu_1$ (C)	–	1.97	1.31	1.48
CH_2CHOH	8	$\eta_2\mu_2$ (C,C)	–	2.14, 2.16	1.40	1.48
$CHCH_2OH$	9	$\eta_1\mu_2$ (C)	–	2.10, 2.08	1.44	1.51
CH_3CO	10	$\eta_1\mu_1$ (C)	–	2.05	1.22	1.50
CH_2CHO	11	$\eta_1\mu_1$ (C)	–	2.13	1.29	1.45
$CHCH_2O$	12	$\eta_2\mu_3$ (C,O)	2.04	2.08, 2.09	1.39	1.50
CH_2COH	13	$\eta_2\mu_3$ (C,C)	–	2.09, 2.13	1.35	1.47
$CHCHOH$	14	$\eta_2\mu_3$ (C,C)	–	2.08, 2.12	1.38	1.48
CCH_2OH	15	$\eta_1\mu_3$ (C)	–	2.02	1.42	1.49
CH_2CO	16	$\eta_2\mu_2$ (C,C)	–	2.09, 2.06	1.21	1.49
$CHCHO$	17	$\eta_1\mu_2$ (C)	–	2.11	1.27	1.43
CCH_2O	18	$\eta_2\mu_3$ (C,O)	2.15	1.94	1.42	1.54
$CHCOH$	19	$\eta_2\mu_3$ (C,C)	–	2.13, 2.08, 1.94	1.33	1.41
$CCHOH$	20	$\eta_1\mu_3$ (C)	–	1.99, 2.09	1.34	1.41
$CHCO$	21	$\eta_2\mu_3$ (C,C)	–	2.08, 2.06	1.21	1.45
$CCHO$	22	$\eta_1\mu_3$ (C)	–	2.01	1.23	1.49
$CCOH$	23	$\eta_2\mu_3$ (C,C)	–	2.01, 1.96	1.31	1.39
CCO	24	$\eta_1\mu_3$ (C)	–	2.03	1.18	1.34

Note: C–H bond lengths are 1.10 ± 0.02 Å and O–H bond lengths are 0.98 ± 0.02 Å.

The transition state for C–O bond cleavage having the lowest energy corresponds to reaction of adsorbed 1-hydroxyethylidene (CH_3COH) species. The geometry for this transition state is shown in Fig. 3 (species 2) and the transition state energy is 42 kJ/mol with respect to gas-phase ethanol. The C–O, C–Pt, and O–Pt distances are 2.13, 1.98, and 2.11 Å, respectively. The 1-hydroxyethylidene (CH_3COH) reactant species is initially adsorbed on a bridge site ($\eta_1\mu_2$), which is 51 kJ/mol less stable than atop adsorption ($\eta_1\mu_1$). The bridge bonded 1-hydroxyethylidene ($\eta_1\mu_2$) species is an intermediate between the atop bonded 1-hydroxyethylidene ($\eta_1\mu_1$) species and its C–O bond cleavage transition state. Products of the C–O bond cleavage reaction are ethylidyne (CH_3C) and hydroxyl species. These species adsorb on threefold hollow and atop sites, respectively, and they are the most stable C–O bond cleavage products (−38 kJ/mol).

The transition state with the lowest energy for cleavage of the C–C bond corresponds to reaction of the adsorbed ketenyl (CHCO) species. The transition state is shown in Fig. 3 (species 14) and the energy is 4 kJ/mol with respect to gas-phase ethanol. The C–C bond length in this transition state is 2.01 Å. The C–Pt bond distances at the transition state are 1.99 and 1.96 Å for the methylidyne (CH) and CO fragments, respectively. The methylidyne (CH) and CO species adsorb on threefold sites, and they are the most stable C–C cleavage products (−144 kJ/mol). Preferential adsorption of CO on threefold sites is in agreement with reported DFT studies, although experimental results indicate CO adsorption occurs on bridge and atop sites [31].

In general, it is possible that transition state species for cleavage of C–C and C–O bonds may be sensitive to unit cell dimensions, due to lengthening of these chemical bonds in bond cleavage reactions. In addition, larger molecules (such as the more highly hydrogenated species in the present study) may be sensitive to unit cell dimensions. Therefore, convergence of the energetics for selected species was tested using a 3×3 unit cell. Generally, no significant effects were found of increasing the unit cell size from 2×2 to 3×3, except for C–O bond cleavage of 2-hydroxyethyl (CH_2CH_2OH) species. The transition state on a 2×2 unit cell is shown in Fig. 3 (species 1) and the transition state energy is 192 kJ/mol. This bond cleavage reaction requires an ensemble of four Pt atoms. We have found an alternative reaction path that requires only two adjacent Pt atoms on a 3×3 slab, and the transition state is approximately 90 kJ/mol lower in energy. This reaction path has been previously reported [2].

Figs. 4 and 5 show schematic potential energy diagrams for cleavage of C–O and C–C bonds in various species adsorbed on Pt(111). The energies of all species in this diagram are relative to gas-phase ethanol and the clean slab(s). The solid curves in these figures correspond to cleavage of C–O and C–C bonds by the 15 transition states listed in Table 2 and shown in Fig. 3. Various other pathways for C–O and C–C bond cleavage can be identified as being uncompetitive with cleavage of the C–O bond through the 1-hydroxyethylidene (CH_3COH) intermediate or with cleavage of the C–C bond through the ketenyl (CHCO) intermediate. Specifically, the reactants and/or products of these uncompetitive pathways have energies that are already higher than the energies of the transition states for the more favorable pathways. These uncompetitive pathways are depicted by vertical solid lines in Figs. 4 and 5.

In addition to the 15 transition states listed in Table 2 and the uncompetitive pathways noted above, cleavage of the C–O and the C–C bonds may also take place through the other adsorbed intermediates shown in Fig. 2. To address whether C–O or C–C bond cleavage through these other adsorbed species may be competitive with the most favorable pathways identified in Figs. 4 and 5, we estimate the energies of the transition states for these additional possible pathways from the energies of the known transition states of Table 2. In this respect, we use a Brønsted–Evans–Polanyi type correlation to relate the energy of the transition state to the energy of the products for an exothermic reaction. Accordingly, Fig. 6 is a plot of transition state energies versus the corresponding final state energies for 14 of the 15 transition states of Table 2, where each surface reaction is defined in the exothermic direction. The 2-hydroxyethyl (CH_2CH_2OH)

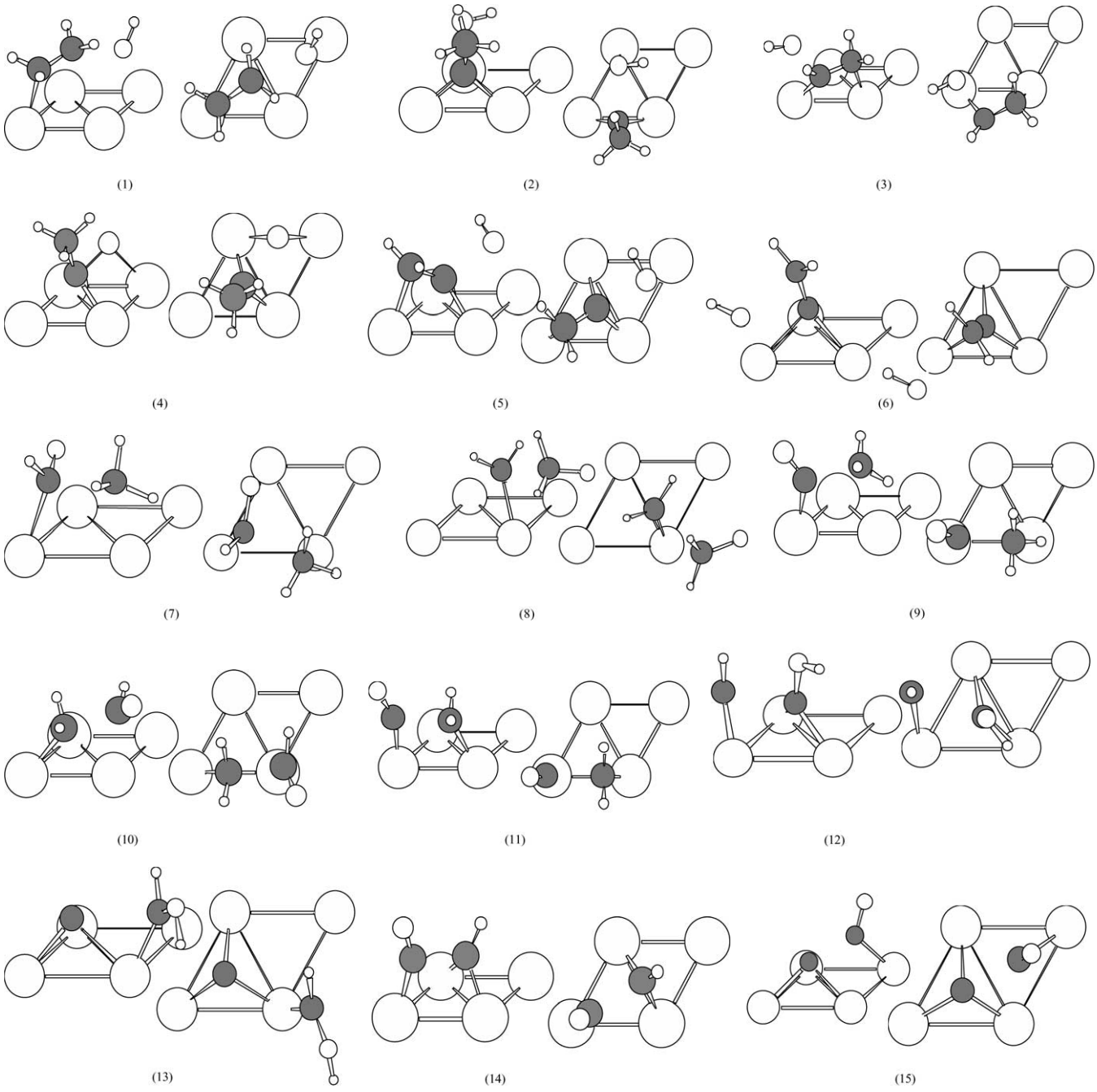

Fig. 3. Side and top views for transition states: (1) 2-hydroxyethyl (CH_2CH_2OH), (2) 1-hydroxyethylidene (CH_3COH), (3) hydroxyethylene (CH_2CHOH), (4) acetyl (CH_3CO), (5) 1-hydroxyvinyl (CH_2COH), (6) hydroxyethylidyne (CCH_2OH), (7) acetaldehyde (CH_3CHO), (8) ethylene oxide (CH_2CH_2O), (9) acetyl (CH_3CO), (10) formylmethyl (CH_2CHO), (11) ketene (CH_2CO), (12) hydroxyacetylene (CHCOH), (13) hydroxyvinylidene (CCHOH), (14) ketenyl (CHCO), and (15) CCO. The large white circles represent Pt atoms, gray medium circles represent C atoms, white medium circles represent O atoms, and the small white circles represent H atoms.

C–O bond cleavage transition state is not plotted because of the aforementioned coverage effects.

We note here that we search for a correlation such as that given in Fig. 6 for practical rather than for fundamental purposes. In particular, the purpose of such a correlation is to determine whether other transition states for cleavage of C–C and C–O bonds (that we have not yet studied in detail) are likely to exist that have energies lower than those that we have already identified from detailed DFT calculations. Transition states with energies that are predicted to be comparable or lower than those values for the lowest energy transition states we have already identified (within the error estimate for the transition state energy correlation) would warrant further detailed studies by DFT calculations.

The energies of the transition states (TS) and final states (FS) are relative to the energies of the corresponding ini-

Table 4
Bond lengths (Å) from DFT calculations for transition states species on Pt(111)

Intermediate	Stoichiometry	Fig. 3 species	O–Pt	C–Pt	C–O	C–C
		C–O cleavage				
2-Hydroxyethyl	CH_2CH_2OH	1	2.14	2.19	2.12	1.44
1-Hydroxyethylidene	CH_3COH	2	2.11	1.98	2.13	1.49
Hydroxyethylene	CH_2CHOH	3	2.21	2.11, 2.21	1.91	1.46
Acetyl	CH_3CO	4	2.14, 2.09	2.04, 1.94	1.93	1.48
1-Hydroxyvinyl	CH_2COH	5	2.35	2.21, 1.97	2.01	1.43
Hydroxyethylidyne	CCH_2OH	6	2.24	1.99, 2.03	2.39	1.38
		C–C cleavage				
Acetaldehyde	CH_3CHO	7	2.16	2.04, 2.30	1.29	2.01
Ethylene oxide	CH_2CH_2O	8	2.22	2.04, 2.71	1.29	2.13
Acetyl	CH_3CO	9	–	2.62, 1.97	1.20	1.98
Formylmethyl	CH_2CHO	10	–	2.06, 2.21	1.22	1.91
Ketene	CH_2CO	11	–	2.01, 1.91	1.18	2.05
Hydroxyacetylene	CHCOH	12	–	2.03, 1.90	1.34	2.13
Hydroxyvinylidene	CCHOH	13	–	1.92, 2.00	1.31	2.50
Ketenyl	CHCO	14	–	1.99, 1.96	1.19	2.01
	CCO	15	–	1.97, 2.04	1.20	1.75

Note: C–H bond lengths are 1.10 ± 0.02 Å and O–H bond lengths are 0.98 ± 0.02 Å.

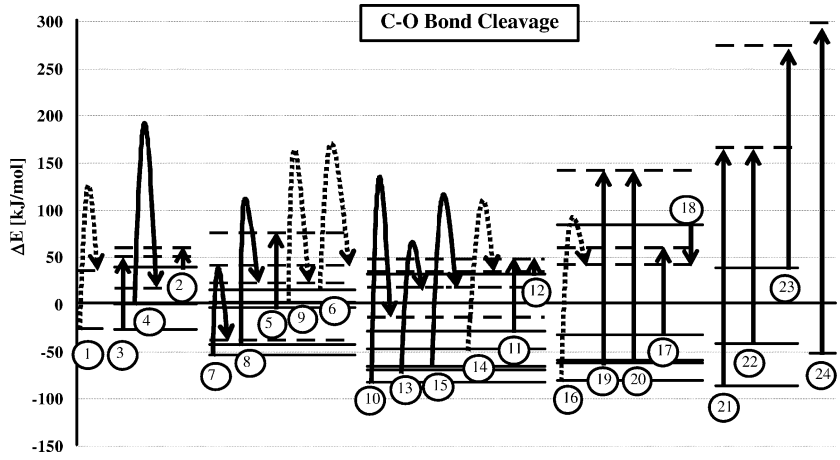

Fig. 4. Reaction energy diagram for C–O bond cleavage reactions relative to gas-phase ethanol and clean slabs. Bond cleavage products and removed H atoms are adsorbed on separate slabs. Solid curves represent calculated transition states. Dashed curves represent estimated transition states. Vertical solid lines represent uncompetitive bond cleavage reactions. Species labels are circled and correspond to species in Table 2 and Fig. 2.

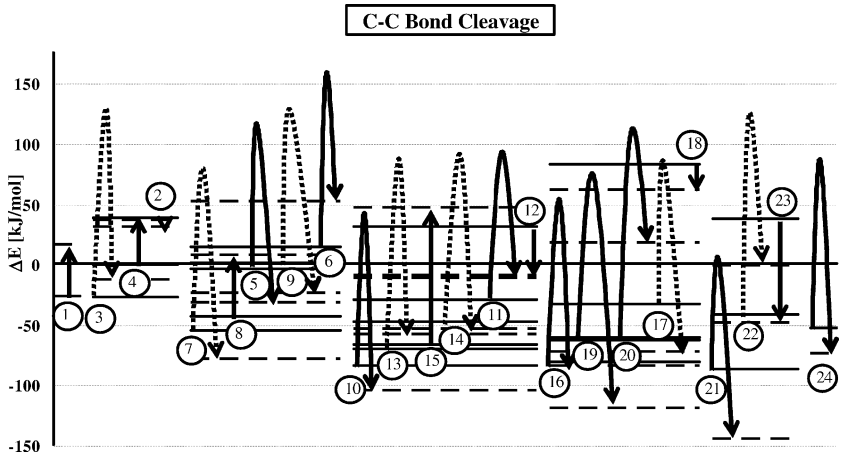

Fig. 5. Reaction energy diagram for C–C bond cleavage reactions relative to gas-phase ethanol and clean slabs. Bond cleavage products and removed H atoms are adsorbed on separate slabs. Solid curves represent calculated transition states. Dashed curves represent estimated transition states. Vertical solid lines represent uncompetitive bond cleavage reactions. Species labels are circled and correspond to species in Table 2 and Fig. 2.

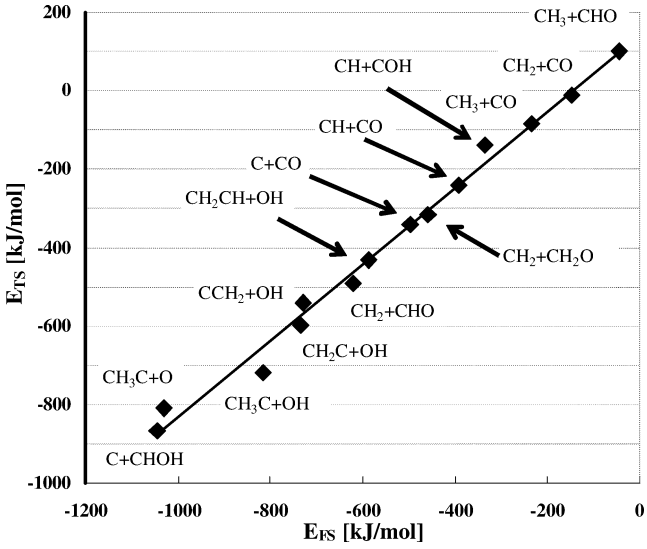

Fig. 6. Correlation plot for C–O and C–C bond cleavage reactions calculated from DFT. Final state (E_{FS}) and transition state (E_{TS}) energies are relative to initial state gas-phase energies. Reaction direction is defined in the exothermic direction. The linear regression equation is E_{TS} (kJ/mol) = $0.97E_{FS}$ (kJ/mol) + 140 kJ/mol and the standard error is 31 kJ/mol. The 2-hydroxyethyl (CH_2CH_2OH) C–O bond cleavage transition state is not included because of coverage effects.

tial state gas-phase species (shown in Table 1). For example, the surface reaction for cleavage of the C–O bond in 1-hydroxyethylidene (CH_3COH) is endothermic (Table 2). Therefore, the initial state is ethylidyne (CH_3C) and hydroxyl (OH) species and the final state is the 1-hydroxyethylidene (CH_3COH) surface species. The final state energy relative to the gas-phase initial state energy, shown in reaction (1), is calculated from data in Tables 1 and 2:

$$CH_3C(g) + OH(g) + 2H^* + {}^* \rightarrow CH_3COH^* + 2H^*, \qquad (1)$$

$$E_{FS} = -55 - 761 \text{ (kJ/mol)},$$

$$E_{FS} = -816 \text{ kJ/mol}.$$

The transition state energy (relative to the gas-phase initial state) is calculated from the calculated final state energy and activation energies (Table 2):

$$E_{TS} = -816 + (42 - (-55)) \text{ (kJ/mol)},$$

$$E_{TS} = -719 \text{ kJ/mol}.$$

Similar correlations have been reported by Nørskov [32]. The linear regression equation for Fig. 6 is reported in the figure caption, and this correlation is used to estimate transition state energies of remaining C–O and C–C bond cleavage pathways. The standard error of the fitted data is 31 kJ/mol. The estimated transition state energies for these additional possible C–O and C–C bond cleavage pathways are represented by dashed curves in Figs. 4 and 5, respectively. As indicated above, the correlation of Fig. 6 is used only for empirical purposes in the present paper to estimate whether additional transition state states should be investigated in detail. It is interesting to note, however, that the slope of this correlation suggests that the transition states for these C–C and C–O reactions resemble the final states (written in the exothermic direction).

4. Discussion

The results from the DFT calculations of the present study indicate that hydroxyethyl species are more stable than ethoxy species on Pt(111). A similar stability trend has been found for hydroxymethyl and methoxy species on Pt(111) [18]. Hydroxyalkyl species bind through C atoms and alkoxy species bind through the O atom on atop sites. For example, the 1-hydroxyethyl (CH_3CHOH) and 2-hydroxyethyl (CH_2CH_2OH) species are more stable than ethoxy (CH_3CH_2O) surface species by 66 and 39 kJ/mol, respectively. Thus, cleavage of C–H bonds in species derived from ethanol leads to more strongly adsorbed species on Pt(111), compared to cleavage of O–H bonds.

Most species follow gas-phase bond order rules, wherein C is tetravalent and O is divalent, except for the 1-hydroxyethylidene (CH_3COH; $\eta_1\mu_1$), CCH_2O, hydroxyacetylene (CHCOH), hydroxyvinylidene (CCHOH), hydroxyethynyl (CCOH), and CCO species. According to these rules, the 1-hydroxyethylidene (CH_3COH) species would be expected to adsorb preferentially in a bridge site. However, the 1-hydroxyethylidene ($\eta_1\mu_1$) species adsorbed on atop sites is more stable by 15 kJ/mol. The lengths of the C–Pt and C–O bonds (1.97 and 1.31 Å, respectively) are shorter in atop adsorption compared to bridge adsorption (2.17 and 1.36 Å, respectively). Thus, the C–Pt and the C–O bonds appear to develop some double-bond character in the $\eta_1\mu_1$ adsorption mode.

The transition state for C–O bond cleavage having the lowest energy, as shown in Fig. 4, involves cleavage of this bond in adsorbed 1-hydroxyethylidene (CH_3COH) species. The bridge-bonded 1-hydroxyethylidene (CH_3COH) species is a reactive precursor for C–O bond cleavage because the O and C atoms are close to the surface. In addition, the low energy for this transition state may be related to the low energy of the ethylidyne (CH_3C) and hydroxyl species formed in this C–O bond cleavage step. In contrast to the high reactivity of adsorbed 1-hydroxyethylidene (CH_3COH) species, cleavage of the C–O bond in adsorbed CO on Pt(111) is unlikely, since Morikawa et al. have reported large transition state barriers for C–O bond cleavage (approximately 420 kJ/mol relative to adsorbed CO) [33]. Accordingly, CO desorption is more likely than decomposition, since the CO-binding energy is approximately 180 kJ/mol [18,34].

The adsorbed ketenyl (CHCO) species is the most stable species derived from ethanol, and it leads to the lowest energy transition state for cleavage of the C–C bond, as shown in Fig. 5. The low energy for this transition state may again be related to the high stability of the adsorbed methylidyne (CH) and CO species formed in this C–C bond cleavage step.

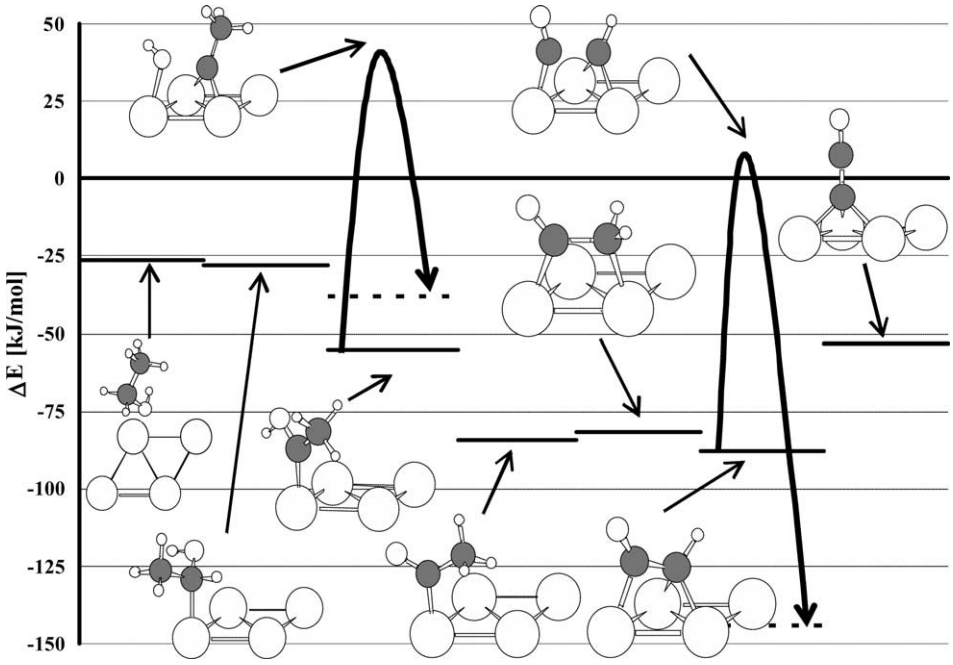

Fig. 7. Reaction energy diagram for ethanol reactions on Pt(111). The reference state is gas-phase ethanol and clean slab(s). Removed H atoms and bond cleavage products are each adsorbed on separate slabs. Solid curves represent bond cleavage reactions. Insets show views of stable and transition state species. The large white circles represent Pt atoms, gray medium circles represent C atoms, white medium circles represent O atoms, and the small white circles represent H atoms.

Fig. 7 shows a simplified potential energy diagram of the stabilities and reactivities of dehydrogenated species derived from ethanol on Pt(111). Only the most stable species within each isomeric set and the most stable transition states for C–O and C–C bond cleavage are consolidated in this schematic potential energy diagram. Views of adsorbed species and transition states are shown in the insets. The relative rates of C–O versus C–C bond cleavage are controlled by the energetics of the transition states that control these processes. It can be seen from Fig. 7 that C–O bond cleavage occurs on more highly hydrogenated species compared to C–C bond cleavage. Thus, low hydrogen partial pressures appear to favor C–C bond cleavage reactions. If it is assumed that hydrogenation/dehydrogenation steps are quasiequilibrated compared to C–O and C–C bond cleavage steps, then the rates of C–O and C–C bond cleavage are controlled according to transition state theory by lumped steps (2) and (3) below, respectively:

$$CH_3CH_2OH(g) + {}^{*} \overset{\text{C–O}}{\rightleftarrows} [CH_3COH^{*}]^{\neq} + H_2(g), \qquad (2)$$

$$CH_3CH_2OH(g) + {}^{*} \overset{\text{C–C}}{\rightleftarrows} [CHCO^{*}]^{\neq} + \tfrac{5}{2}H_2(g). \qquad (3)$$

According to the DFT results listed in Table 2, and using the DFT value of 86 kJ/mol for the energy change corresponding to the desorption of H_2 from Pt(111), the energy changes for lumped steps (2) and (3) are equal to 128 and 219 kJ/mol, respectively. Therefore, C–C bond cleavage has a higher activation energy and is thus favored at higher temperatures compared to C–O bond cleavage. The rates of C–O and C–C bond cleavage on Pt(111) are given from transition state theory by

$$r_{\text{C–O}} = \frac{k_B T}{h} \exp\left(-\frac{\Delta G_2^{o\neq}}{RT}\right) \frac{P_{CH_3CH_2OH}}{P_{H_2}^{1}} \theta_{*},$$

$$r_{\text{C–C}} = \frac{k_B T}{h} \exp\left(-\frac{\Delta G_3^{o\neq}}{RT}\right) \frac{P_{CH_3CH_2OH}}{P_{H_2}^{5/2}} \theta_{*},$$

where $\Delta G_i^{o\neq}$ represents the standard Gibbs free energy change of reaction i, k_B is the Boltzmann constant, R is the gas constant, h is the Planck constant, and P_i are partial pressures (in units of atm). The enthalpy change for each reaction is estimated to be equal to the value of the energy change determined from DFT calculations, since thermal and zero-point energy corrections are small compared to the accuracy of the DFT calculations. To estimate the standard entropy change for each lumped reaction, we assume that reaction leads (i) to the loss of gas-phase translational entropy for ethanol (calculated using the standard translational entropy of a gaseous molecule with 3 degrees of freedom), (ii) to the gain of entropy for the corresponding amount of gas-phase hydrogen (from the tabulated gas phase entropy at 298 K, and thermal corrections calculated using the tabulated heat capacity), and (iii) to an adsorbed transition state that has the local entropy (i.e., rotation and vibration) of the corresponding C_2H_xO species. Local entropies of species are calculated from the difference between total entropies and three-dimensional translational entropies of gaseous species:

$$S_{\text{loc}} = S_{\text{tot}} - S_{\text{trans, 3D}}.$$

These values are calculated directly for tabulated gas-phase species (i.e., CH_3CH_2OH, CH_3CHO, CH_2CO, and CO), and averages of these values are used to estimate local entropies of other species that are not listed in standard tabulations (i.e., CH_3CH_2O, CH_3CO, and CHCO).

The values of the standard Gibbs free energy changes for reactions (2) and (3) become equal (i.e., 150 kJ/mol) at about 500 K. At the higher temperature of 550 K, the values of the standard Gibbs free energy changes for reactions (2) and (3) are equal to 153 and 145 kJ/mol, respectively. Accordingly, the values of the rate constants at this temperature for cleavage of C–O and C–C bonds are calculated to be equal to 3×10^{-2} and 2×10^{-1} s^{-1}, respectively. Therefore, the results from the DFT calculations of the present study suggest that the rate constant for C–C bond cleavage in ethanol on Pt(111) should be higher than the rate constant for C–O bond cleavage at temperatures higher than about 500 K. These predictions are in agreement with experimental data for ethanol conversion on supported Pt catalysts at temperatures above 490 K, where turnover frequencies for C–C bond cleavage (H_2 and CO) are higher than for C–O bond cleavage (ethane) [2]. The results from our DFT calculations are also in general agreement with the recent report that Pt-based catalysts are effective for the selective cleavage of C–C bonds compared to C–O bonds in oxygenated hydrocarbons at temperatures near 500 K, i.e., Pt-based catalysts lead to selective production of H_2 (in contrast to production of alkanes) during reforming of oxygenated hydrocarbons at temperatures near 500 K [1].

In the present study we have not investigated transition states for cleavage of C–H and O–H bonds in species derived from ethanol on Pt(111). Theoretical calculations have been conducted for C–H and O–H bond cleavage reactions in methanol [18]. The rate-limiting step for methanol dehydrogenation appears to be O–H bond cleavage, but the transition state energies are similar for O–H versus C–H bond cleavage. The transition state energies for C–H and O–H bond cleavage are approximately 50–60 kJ/mol relative to gas-phase methanol. Therefore, if the energies of transition states for C–H and O–H bond cleavage in ethanol are similar to the values for methanol, then these steps may not be quasiequilibrated with respect to C–C and C–O bond cleavage reactions for ethanol reforming on Pt(111) at low temperatures. At temperatures near 500 K, however, experimental studies of gas-phase ethanol decomposition over Pt-based catalysts show that acetaldehyde is equilibrated with ethanol, compared to the slower rates of formation of CO and CH_4 by C–C bond cleavage [2].

We now use transition state theory with the DFT results of the present study to estimate and compare the rate of C–C bond cleavage in ethanol with the rate of C–C bond cleavage in ethane on Pt(111). In particular, the adsorbed C_2H_x species derived from ethane on Pt(111) with the lowest activation energy barrier for cleavage of the C–C bond is adsorbed ethylidene (CH_3CH), and this activation energy barrier is 106 kJ/mol [17]. The electronic energy associated with the formation of this transition state (and adsorbed H atoms) from ethane is equal to 125 kJ/mol (compared to the value of 4 kJ/mol for C–C cleavage in adsorbed ketenyl (CHCO) species). Using the DFT value of 86 kJ/mol for the energy change corresponding to the desorption of H_2 from Pt(111), the energy change for lumped step (4) is equal to 211 kJ/mol:

$$C_2H_6(g) + {}^* \overset{\text{C–C}}{\rightleftarrows} [CHCH_3^*]^{\neq} + H_2(g). \tag{4}$$

The rate of C–C bond cleavage from ethane on Pt(111) is given from transition state theory by

$$r_{\text{C–C}} = \frac{k_B T}{h} \exp\left(-\frac{\Delta G_4^{0\neq}}{RT}\right) \frac{P_{C_2H_6}}{P_{H_2}^1} \theta_*.$$

Using the same assumptions described above to estimate the standard entropy change for lumped reaction (4), we calculate that value of the standard Gibbs free energy change for reaction (4) is equal to 228 kJ/mol at about 550 K. Accordingly, the value of the rate constant at this temperature for cleavage of C–C bond in ethane is calculated to be equal to 3×10^{-9} s^{-1}. Therefore, it is apparent that the rate constant for C–C bond cleavage in ethanol (i.e., 2×10^{-1} s^{-1}) should be much faster than the rate constant for C–C bond cleavage in ethane (i.e., 3×10^{-9} s^{-1}) on Pt(111) at temperatures near 550 K. In agreement with this conclusion, it is known from the homogeneous catalysis literature that metal-catalyzed cleavage of C–C bond in aldehydes takes place readily at temperatures lower than 500 K [35,36].

5. Conclusions

Results from periodic, self-consistent DFT calculations were used to determine the relative stabilities of various species derived from ethanol on Pt(111). Transition states for C–C and C–O bond cleavage pathways were investigated for selected intermediates, i.e., for the most stable intermediates and for intermediates leading to exothermic bond cleavage reactions. The 1-hydroxyethylidene and ketenyl species have the lowest energy transition states for C–O and C–C bond cleavage, respectively. In addition, products of these species (ethylidyne, hydroxyl, methylidyne, and CO) have the most stable energies. From the DFT results of this study, it can be estimated using transition state theory that the rate constant for C–C bond cleavage in ethanol is faster than for C–O bond cleavage on Pt(111) at temperatures higher than about 550 K. This prediction is in agreement with experimental results for ethanol decomposition and ethanol reforming on Pt catalysts at these temperatures. In addition, the calculated value of the rate constant for C–C bond cleavage in ethanol at temperatures near 550 K is much higher than for C–C bond cleavage in ethane. Similarly, the rate of C–O bond cleavage in ethanol is expected to be much higher than for C–O bond cleavage in carbon monoxide on Pt(111).

Acknowledgments

Rafael Alcalá acknowledges a Ford Predoctoral Fellowship from the National Research Council. In addition, we acknowledge funding from the National Science Foundation and the Materials Research Science and Engineering Center (Nanostructured Materials and Interfaces) at the University of Wisconsin. We thank BP-Amoco for an equipment grant. Part of the calculations were performed at DOE-BES NERSC and NPACI supercomputing facilities. We thank Jeff Greeley for valuable discussions regarding DFT calculations.

References

[1] R.D. Cortright, R.R. Davda, J.A. Dumesic, Nature 418 (2002) 964.
[2] K.I. Gursahani, R. Alcala, R.D. Cortright, J.A. Dumesic, Appl. Catal. A 222 (2001) 369.
[3] C. Panja, N. Saliba, B.E. Koel, Surf. Sci. 395 (1998) 248.
[4] M.A. Vannice, W. Erley, H. Ibach, Surf. Sci. 254 (1991) 1.
[5] B.A. Sexton, K.D. Rendulic, A.E. Hughes, Surf. Sci. 121 (1982) 181.
[6] K.D. Gibson, L.H. Dubois, Surf. Sci. 233 (1990) 59.
[7] M.K. Rajumon, M.W. Roberts, F. Wang, P.B. Wells, J. Chem. Soc., Fararaday Trans. 94 (1998) 3699.
[8] Y. Cong, V. van Spaedonk, R.I. Masel, Surf. Sci. 385 (1997) 246.
[9] R.W. McCabe, C.L. DiMaggio, R.J. Madix, J. Phys. Chem. 89 (1985) 854.
[10] S. Schauermann, J. Hoffmann, V. Johánek, J. Hartmann, J. Libuda, H.-J. Freund, Angew. Chem., Int. Ed. 41 (2002) 2532.
[11] J. Greeley, J.K. Nørskov, M. Mavrikakis, Annu. Rev. Phys. Chem. 53 (2002) 319.
[12] B. Hammer, L.B. Hansen, J.K. Nørskov, Phys. Rev. B: Condens. Matter Mater. Phys. 59 (1999) 7413.
[13] D.H. Vanderbilt, Phys. Rev. B: Condens. Matter Mater. Phys. 41 (1990) 7892.
[14] J.A. White, D.M. Bird, Phys. Rev. B: Condens. Matter Mater. Phys. 50 (1994) 4954.
[15] J.P. Perdew, J.A. Chevary, S.H. Vosko, K.A. Jackson, M.R. Pederson, D.J. Singh, C. Fiolhais, Phys. Rev. B: Condens. Matter Mater. Phys. 46 (1992) 6671.
[16] G. Kresse, J. Furthmuller, Comput. Mater. Sci. 6 (1996) 15.
[17] R.M. Watwe, R.D. Cortright, J.K. Nørskov, J.A. Dumesic, J. Phys. Chem. B 104 (2000) 2299.
[18] J. Greeley, M. Mavrikakis, J. Am. Chem. Soc. 124 (2002) 7193.
[19] R.P. Elliott, Constitution of Binary Alloys, First Supplement, McGraw–Hill, New York, 1965.
[20] B.E. Spiewak, R.D. Cortright, J.A. Dumesic, J. Catal. 176 (1998) 405.
[21] S.B. Sharma, J.T. Miller, J.A. Dumesic, J. Catal. 148 (1994) 198.
[22] A. Alavi, P. Hu, T. Deutsch, P.L. Silvestrelli, J. Hutter, Phys. Rev. Lett. 80 (1998) 3650.
[23] R.M. Watwe, H.S. Bengaard, J.R. Rostrup-Nielsen, J.A. Dumesic, J.K. Nørskov, J. Catal. 189 (2000) 16.
[24] G. Mills, H. Jónsson, G.K. Schenter, Surf. Sci. 324 (1995) 305.
[25] G. Henkelman, B. Uberuaga, H. Jónsson, J. Chem. Phys. 13 (2000) 9901.
[26] G. Henkelman, H. Jónsson, J. Chem. Phys. 113 (2000) 9978.
[27] D.R. Lide (Ed.), CRC Handbook of Chemistry and Physics, 3rd electronic ed., CRC Press, Boca Raton, FL, 2000.
[28] J. Park, R.S. Zhu, M.C. Lin, J. Chem. Phys. 117 (2002) 3224.
[29] R. Alcalá, J. Greeley, M. Mavrikakis, J.A. Dumesic, J. Chem. Phys. 116 (2002) 8973.
[30] M. Mavrikakis, M.A. Barteau, J. Mol. Catal. A: Chem. 131 (1998) 135.
[31] P.J. Feibelman, B. Hammer, J.K. Nørskov, F. Wagner, M. Scheffler, R. Stumpf, R. Watwe, J. Dumesic, J. Phys. Chem. B 105 (2001) 4018.
[32] J.K. Nørskov, T. Bligaard, A. Logadottir, S. Bahn, L.B. Hansen, M. Bollinger, H. Bengaard, B. Hammer, Z. Sljivancanin, M. Mavrikakis, Y. Xu, S. Dahl, C.J.H. Jacobsen, J. Catal. 209 (2002) 275.
[33] Y. Morikawa, J.J. Mortensen, B. Hammer, J.K. Nørskov, Surf. Sci. 386 (1997) 67.
[34] S.G. Podkolzin, J. Shen, J.J. de Pablo, J.A. Dumesic, J. Phys. Chem. B 104 (2000) 4169.
[35] C.M. Beck, S.E. Rathmill, Y.J. Park, J.Y. Chen, R.H. Crabtree, L.M. Liable-Sands, A.L. Rheingold, Organometallics 18 (1999) 5311.
[36] F. Abuhasanayn, M.E. Goldman, A.S. Goldman, J. Am. Chem. Soc. 114 (1992) 2520.